CNRS
Centre National de la Recherche Scientifique

INFN
Istituto Nazionale di Fisica Nucleare

Injection system frequency noise budget

VIR-0369A-15

Eleonora Capocasa, Maddalena Mantovani, Matteo Barsuglia,
Eric Genin, Gabriel Pillant, Paolo Ruggi, Bas Swinkels, Matteo Tacca

Issue: 1

Date: September 2, 2015

VIRGO * A joint CNRS-INFN Project
Via E. Amaldi, I-56021 S. Stefano a Macerata - Cascina (Pisa)

Contents

Foreword

The main goal of this note is to describe the methods and tools used for the evaluation of the frequency noise budget of the injection system. The performances of the injection system will be also shown. Since at the time of writing the integration of the injection system is not concluded, these performances will evolve, but the methods and tools will be still valid.

1 Introduction

In order to deliver a beam whose frequency noise meets the requirements necessary to acquire interferometer arms lock (< 1 Hz RMS) [1] two stabilization loops with different bandwidth are used (See Fig.1)[2][3]:

- a first fast pre-stabilization loop ($\sim$ 200 kHz bandwidth) which locks the laser frequency on the input mode cleaner (IMC) length.
- a second loop ($\sim$ 80 Hz bandwidth) which locks the laser frequency on the resonance frequency of a rigid Fabry-Pérot cavity called *reference cavity* (RFC)

In this way the suspended IMC, which is very stable at high frequency (above $\sim$ 10 Hz), is used in that region as a length reference while at low frequency the RFC is used. The error signal for the first loop is generated using the Pound-Drever-Hall (PDH) technique on the beam reflected by the IMC. In the second loop the frequency of the IMC transmitted beam is compared with the RFC length and the PDH signal in reflection is used to control the IMC end mirror and thus the IMC cavity length.

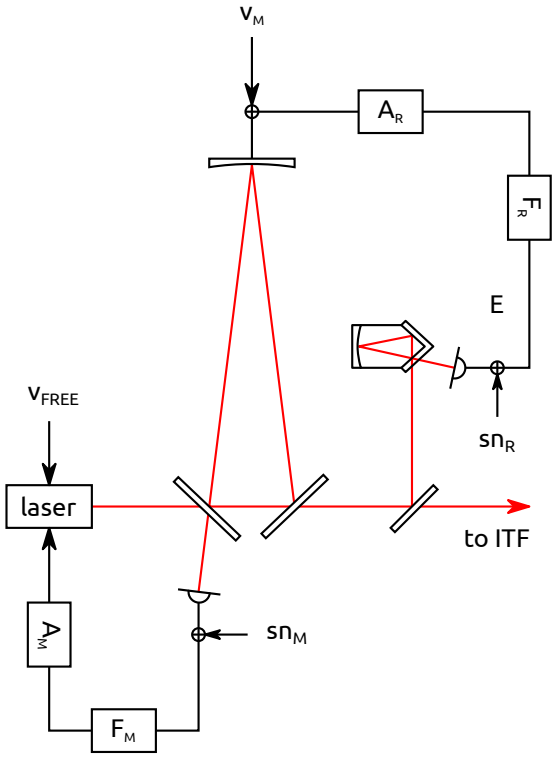

Figure 1: Optical scheme of the two frequency stabilization loops

In Fig.2 a scheme of the two loops is shown. Once the interferometer is locked, a second stage of frequency stabilization (SSFS) is engaged. In this configuration the error signal is provided using the arm as reference.

However our noise analysis is performed on the injection system running in stand-alone configuration. In order to measure the frequency stability of the laser to be sent to the interferometer we measure the PDH error signal in reflection from the RFC which is the result of a comparison between the laser frequency and the RFC length. In this note the noises which affect the RFC error signal are investigated in order to produce a noise budget for the frequency noise of the beam delivered by the injection system to the ITF.

2 Model of the IMC and RFC loops

As a first step we have computed analytically the loop equations to find the projection of each noise on the RFC error signal.

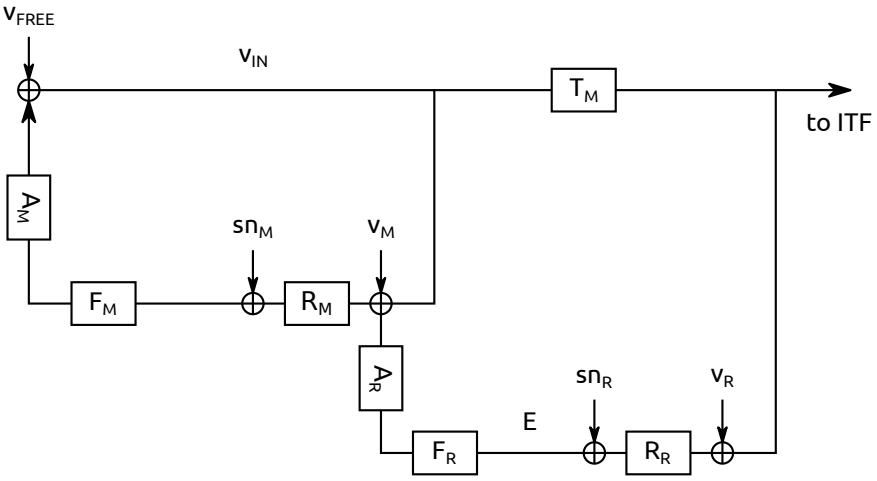

Figure 2: Block scheme of the two frequency stabilization loops

We use the following notation:

- Noises
  - $\nu_{\text{free}}\left[\frac{Hz}{\sqrt{Hz}}\right]$ Free running laser noise
  - $\nu_{\text{R}}\left[\frac{Hz}{\sqrt{Hz}}\right]$ RFC length noise (converted to equivalent frequency noise) [1]
  - $\nu_{\text{M}}\left[\frac{Hz}{\sqrt{Hz}}\right]$ IMC length noise (converted to equivalent frequency noise)
  - $sn_{\text{M}}\ [V]$ sensing noise in the IMC reflection error signal
  - $sn_{\text{R}}\ [V]$ sensing noise in the RFC error signal
- Transfer functions
  - $A_{\text{M}}\ \left[\frac{Hz}{V}\right]$ laser actuator transfer function
  - $F_{\text{M}}\ \left[\frac{V}{V}\right]$ IMC electronic filter transfer function
  - $A_{\text{R}}\ \left[\frac{Hz}{V}\right]$ RFC actuator transfer function
  - $F_{\text{R}}\ \left[\frac{V}{V}\right]$ RFC electronic filter transfer function

[1] When comparing cavity length with laser frequency, length and frequency noise are put on an equal footing. Frequency noise can be transformed in the equivalent length noise and viceversa using $\delta\nu/\nu = \delta L/L$. The conversion factor from m to Hz is $\nu/L = 2 \cdot 10^{12}$

- T_{M} $\left[\frac{Hz}{Hz}\right]$ optical transfer function for the IMC transmission
- R_{M} $\left[\frac{V}{Hz}\right]$ transfer function between the noise entering IMC [Hz] and the PDH demodulated error signal [V]. It includes the optical response of the cavity and the PHD calibration factor $\left[\frac{V}{Hz}\right]$.
- R_{R} $\left[\frac{V}{Hz}\right]$ transfer function between the noise entering RFC [Hz] and the PDH demodulated error signal [V]. It includes the optical response of the cavity (which can be considered flat for the RFC in the frequency region of interest) and the PHD calibration factor.

- E $[V]$ RFC error signal

From the block diagram 2 the following equations can be deduced.

$$E = sn_R + R_{\mathrm{R}}(\nu_R + T_M\nu_{in}) \tag{2.1}$$
$$\nu_{in} = \nu_{\mathrm{free}} + A_M F_M(sn_M + R_M(\nu_M + \nu_{in} + A_R F_R E)) \tag{2.2}$$

then

$$\nu_{in} = \left[\frac{1}{1 - A_M F_M R_M}\right](\nu_{free} + A_M F_M sn_M + A_M F_M R_M \nu_M + A_M F_M R_M A_R F_R E)$$

and

$$E = \left[1 - \frac{T_M A_M F_M R_M A_R F_R R_R}{1 - A_M F_M R_M}\right]^{-1} \tag{2.3}$$
$$\cdot \left[sn_R + R_R\nu_R + (\frac{T_M R_R}{1 - A_M F_M R_M})(\nu_{free} + A_M F_M sn_M) + A_M F_M R_M \nu_M)\right] \tag{2.4}$$

By defining $G_M = A_M F_M R_M$ the pre-stabilization open loop transfer function and $G_R = A_R F_R R_R$ the RFC open loop transfer function, we find

$$E = \left[1 - \frac{T_M G_M G_R}{1 - G_M}\right]^{-1}(sn_R + R_R\nu_R + \frac{T_M R_R}{1 - G_M}\nu_{free} + \frac{T_M R_R G_M}{(1 - G_M)R_M}sn_M + \frac{T_M R_R G_M}{1 - G_M}\nu_M)$$

Assuming a very high gain for the pre stabilization loop in the frequency region of interest ($f < 10$ kHz), that is, considering $G_M \to \infty$ the previous relation becomes:

$$E = \left[\frac{1}{1 + T_M G_R}\right](\mathbf{sn_R} + \frac{T_M R_R}{R_M}\mathbf{sn_M} + R_R\boldsymbol{\nu_R} + T_M R_R\boldsymbol{\nu_M}) \tag{2.5}$$

From Eq.2.5 we read how each noise contributes to the total frequency noise measured by RFC error signal and how the RFC loop affects their projection on the RFC error signal.

2.1 Signal calibration

This calibration factor needed to convert the RFC error signal from Volt to Hz or meter can be obtained measuring the PDH error signal generated during a scan of the laser frequency. It is known that the frequency interval between the two extrema of the PDH signal corresponds to the FWHM of the resonance peak. The FWHM is known and it depends on the cavity length L and on its finesse F:

$$\mathrm{FWHM} = \frac{c}{2\mathrm{LF}} = 5.26 \cdot 10^5 \mathrm{Hz}$$

with L = 0.31 m and F = 920 [5].
This correspondence can be used to convert the error signal acquired as a function of time to a function of frequency.
Since the PDH signal is linear in a small region around the point where it crosses zero, the calibration is found measuring its linear slope(see Fig.3). Another method to find the signal calibration is to measure the open-loop transfer function and compare it with the modeled one, where we have the electronic filter, the actuator and the only free parameter is the optical gain which can be computed from the comparison. The values obtained with these two methods are in agreement within 3%.

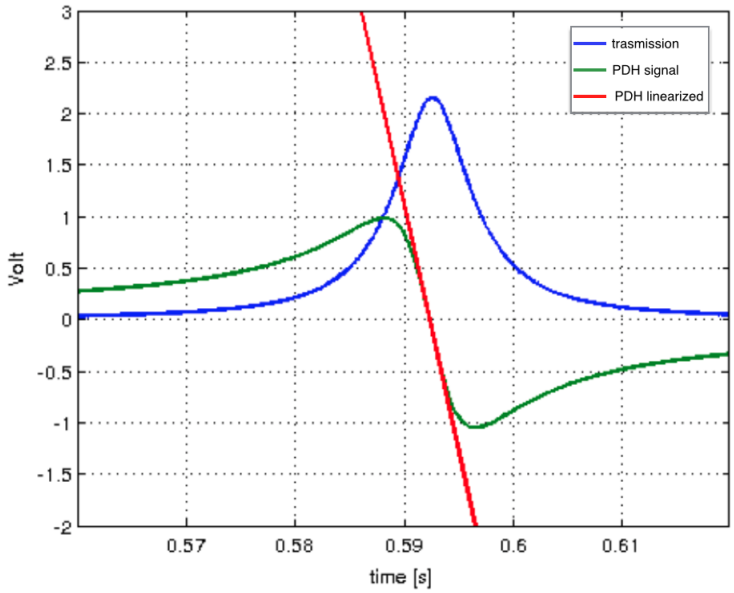

Figure 3: PDH signal and its linearization used to calibrate the RFC error signal

2.2 Transfer functions

The open loop transfer function the RFC, G_M has been measured by means of a noise injection between 10 Hz and 500 Hz. It has been compared with the modeled one which, as already said, is composed by the electronic corrector filter F_M , the mechanical response of the actuator A_M, the optical gain R_M and a pure delay.

Corrector filter[2]: Unity Gain Frequency: 83 Hz

	Freq	Q
real zero	1	0
real zero	5	0
complex zero	11	0.7
complex zero	11	0.7
complex zero	20.5	2
complex zero	28.4	2
real zero	240	0
real pole	0	0
complex pole	2	2
complex pole	5	3
complex pole	20.5	20
complex pole	28.4	20
real pole	800	0
complex pole	2000	0.8

Actuator mechanical response: gain $16 \cdot 10^{-6} m/V$ in DC

	Freq	Q
complex pole	0.667	10

[2]Corrector filter transfer functions are likely to be modified and improved during commissioning activity. Here we reported an example of filter used in the RFC loop which is not the definitive one.

Delay: $800 \cdot 10^{-6}$ s

The comparison between the modeled transfer function and the measured one is shown in Fig4. The two curves agree above 10 Hz where the noise injection has been performed.

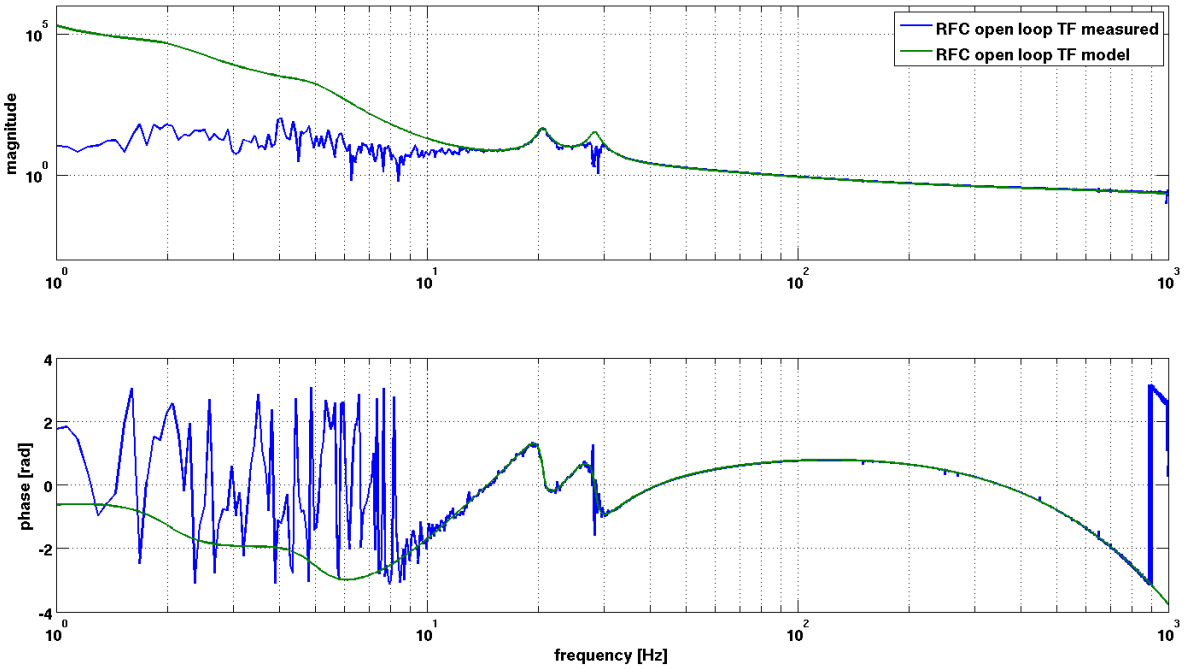

Figure 4: Comparison between the RFC transfer function measured and the theoretical model

3 Sensing noise

The sensing noises of the photodiodes used to lock the reference cavity and the mode-cleaner affect the RFC error signal in the following way (see Eq.2.5):

$$E = \left[\frac{1}{1 + T_M G_R}\right] (\mathbf{sn_R} + \frac{T_M R_R}{R_M} \mathbf{sn_M}) \tag{3.1}$$

since the optical gain R_R of the reference cavity is much smaller than the optical gain of the mode-cleaner R_M, and the two sensing noises are comparable, only the contribution of $\mathbf{sn_R}$ (the sensing noise of the photodiode used to lock the reference cavity), has been taken into account.

3.1 Shot noise

Shot noise is a fundamental noise which stems from the discrete nature of the photons causing an uncertainty in their arrival time on a photo-detector. Being a counting noise, it is governed by Poissonian statistic and, for

a DC signal, it has a frequency-independent spectral density given by[6]

$$S_{shot,DC} = \sqrt{2h\nu P_{in,DC}} \left[\frac{W}{\sqrt{Hz}}\right] \tag{3.2}$$

where $P_{in,DC}$ is the DC power impinging on the photodetector. Shot noise is normally observed in the photocurrent at the output of the photodiode and its value in terms of optical power can be recovered knowing the photodiode responsivity.
We are mainly interested in computing shot noise for a modulated signal. An estimation for it can be found considering a white noise in time with a known spectral density amplitude. If we multiply it by a cosine in the time domain, the spectrum of the noise will remain flat and its amplitude will result reduced of a factor $\frac{1}{\sqrt{2}}$. Thus the shot noise for a demodulated signal can be approximated as [6]

$$S_{shot,AC} = \sqrt{h\nu P_{in,DC}} \left[\frac{W}{\sqrt{Hz}}\right] \tag{3.3}$$

We used this formula to estimate the shot noise of the demodulated RFC error signal. The optical power $P_{in,DC}$ has been found measuring the DC signal in Volt and converting it to Watt using the appropriate calibration k_{DC} which is the product of the photodiode responsivity $\alpha = 0.63[\frac{A}{W}]$ and the resistance $R_{DC} = 7\Omega$. Once we have found $P_{in,DC}$ we put it in (3.3) to find the shot noise for the demodulated signal. In order to compare it with the RFC signal itself it has to be converted in Volt. This has been done using the calibration factor $k_{AC} = \alpha \cdot R_{AC}$ with $R_{AC} = 120\,\Omega$. For an impinging power of 14 mW we have $S_{shot,AC} = 4 \cdot 10^{-9} \left[\frac{V}{\sqrt{Hz}}\right]$.

3.2 Dark and ADC noise

The demodulated signal is digitized by means of an analog-to-digital converter (ADC) which introduces a white noise. This noise has been measured looking at the RFC error signal where the ADC was disconnected. We found

$$n_{ADC} \simeq 2 \cdot 10^{-7} \left[\frac{V}{\sqrt{Hz}}\right] \tag{3.4}$$

The dark noise of the photodiode is due to the random generation of electrons and holes in the junction region of the photodiode which causes a small current to flow even if there is no light impinging on it. We measured the sum of the dark noise and the ADC noise looking at the RFC error signal when there was no light reaching the photodiode, under the assumptions that these noises are independent of the amount of light reaching the photodiode. The noise measured was $n_{sum} \simeq 4.5 \cdot 10^{-7} \frac{V}{\sqrt{Hz}}$. Assuming that dark noise and ADC noise are independent noise, the first can be obtained from the total measured one, knowing the ADC noise:

$$n_{dark} = \sqrt{n_{sum}^2 - n_{ADC}^2} \simeq 4 \cdot 10^{-7} \left[\frac{V}{\sqrt{Hz}}\right] \tag{3.5}$$

The different contributions to the sensing noise and their sum are plotted in Fig.5 along with the RFC error signal.

4 Classical radiation pressure noise

Light impinging on mirrors exerts on them a force known as radiation pressure force. Classical fluctuation in the beam power cause a fluctuation in the radiation pressure force which, moving the mirrors, results in a cavity length noise. Classical radiation pressure has been computed considering that a beam of power P exerts on a mirror a force given by $F = \frac{2P}{c}$; thus the fluctuations in the force are connected to the ones in the power by

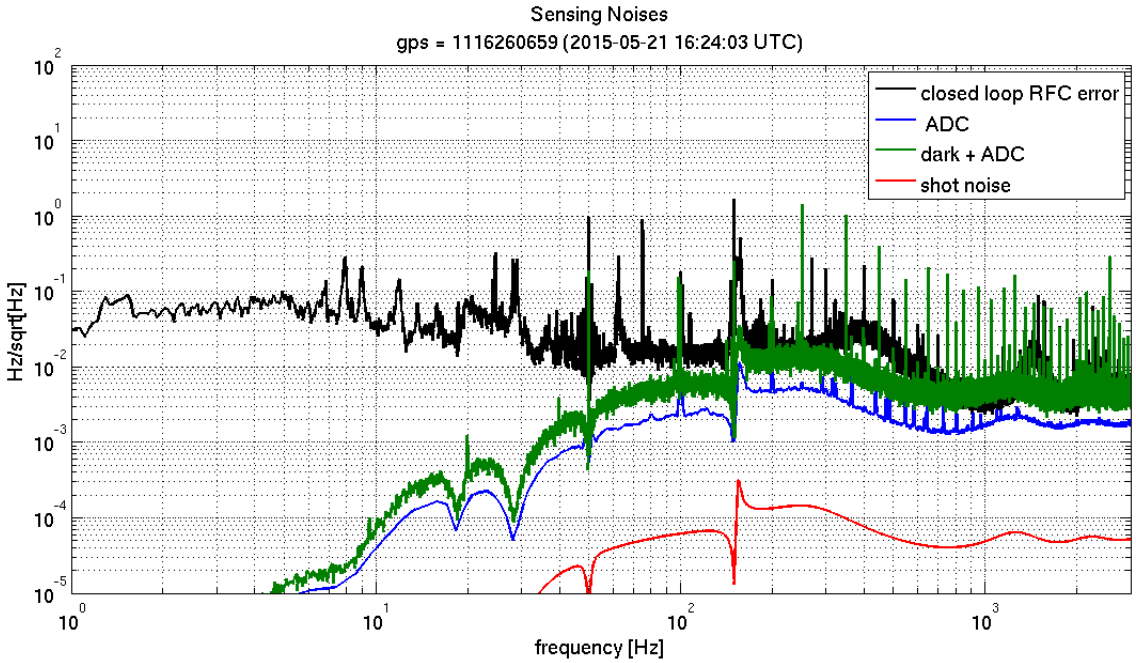

Figure 5: Different contributions to sensing noise and their sum compared with the RFC error sinal

$\Delta F = \frac{2\Delta P}{c}$. From the mirror equation of motion in frequency domain $M\left(-2\pi f^2 + {\omega_0}^2\right)\tilde{x} = \tilde{F}$ we can deduce a relation between the spectral density of the mirror motion and the radiation pressure force:

$$S_x(f) = \frac{2}{cM\left((2\pi f)^2 - (2\pi f_0)^2\right)} \times S_p \tag{4.1}$$

where S_p is the spectral density of the intensity fluctuation of the laser, M is the mirror mass and f_0 is the pendulum resonance frequency.
In order to estimate the fluctuations of the power inside the cavity S_p we made the assumption that the laser relative intensity noise (RIN), that is the laser spectral density divided by its mean power, is the same inside and outside the cavity. Therefore we measured the RIN on the IMC transmitted beam and multiplied it for the estimated value of the power inside the cavity to find S_p. Using the approximated formula $P_{cav} = \frac{Finesse}{\pi} \cdot P_{in}$, for a IMC finesse around 1000 [7] and an input power $P_{in} = 7.6$ W, $P_{cav} \simeq 2.8$ kW.
Since radiation pressure is inversely proportional to the mass, only its effects on the mode cleaner end mirror are taken into account. Its spectrum, compared to the RFC error signal, is plotted in Fig.6. It has been computed using a $M = 3.4$ kg [3] and $f_0 = 0.669$

5 Quantum radiation pressure noise

Fluctuations of the power impinging on the mirror can also be due to the quantum fluctuation in the number of incident photons. As the shot noise, this is another manifestation of the particle nature of light and this two noises can be shown to be interdependent. An estimation for the contribution of this noise can be done starting from the formula for the radiation pressure $\Delta F = \frac{2\Delta P}{c}$ where this time the power fluctuation is determined by

[3] logbook entry 31302

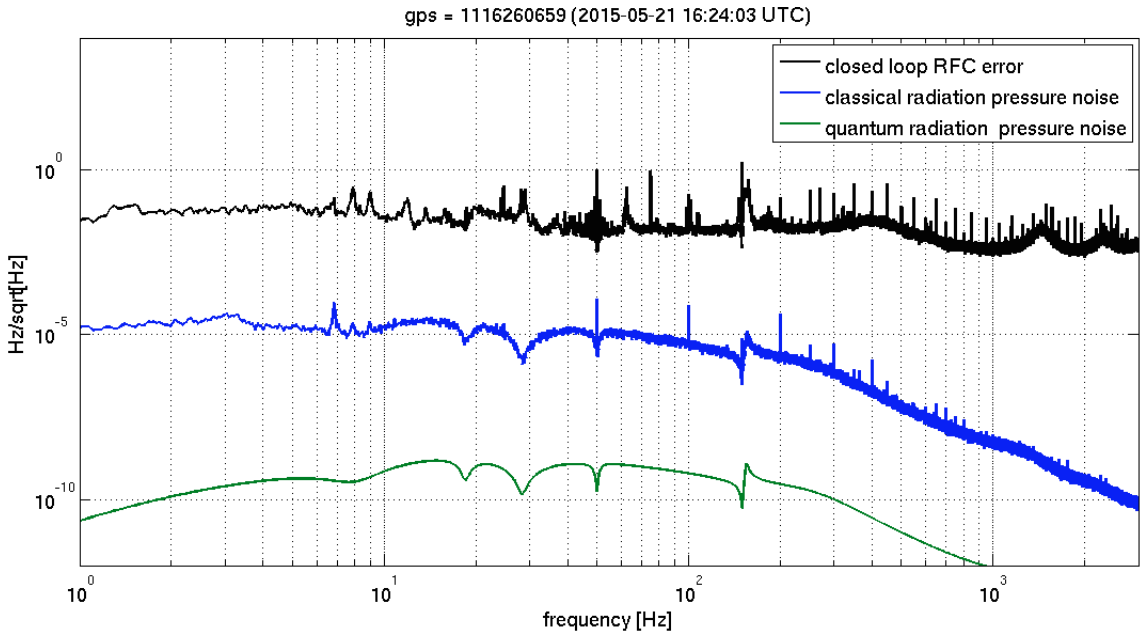

Figure 6: Classical and quantum radiation pressure noise compared with the RFC error signal

the uncertainty on the photon arrival time

$$\Delta P = \frac{\sqrt{h\nu P_{in}}}{T}$$

where T is the observation time. Thus the fluctuating force will be

$$\Delta F = \frac{2}{c}\frac{\sqrt{h\nu P_{cav}}}{T}$$

and its spectral density

$$S_F(f) = \frac{2}{c}\sqrt{2h\nu P_{cav}} \tag{5.1}$$

As in the classical case, we can use the mirror equation of motion to find the spectral density of its displacement. It is found inserting the spectral density of the fluctuating force 5.1 in 4.1:

$$S_x(f) = \frac{2}{cM\left((2\pi f)^2 - (2\pi f_0)^2\right)}\sqrt{2h\nu P_{cav}}$$

Quantum radiation pressure noise spectrum is compared to the classical one in Fig.6

6 Thermal noise

Thermal noise is due to the fact that each vibration mode of the mirrors and of their suspension is randomly excited with an energy proportional to the temperature T of the system. This motion results in a cavity length noise.

The fluctuation-dissipation theorem [8] can be used to deduce the power spectral density of a dissipative force F_{th} acting on a system where $x(t)$ is the position of a mass and $\dot{x}(t) = v(t)$ is the velocity. The equation of motion for the system in frequency domain can always be written as

$$F_{th}(\omega) = Z(\omega)\,\tilde{v}(\omega) \tag{6.1}$$

where $Z(\omega)$ is the impedance. By defining the admittance of the system as $Y(\omega) = Z^{-1}(\omega)$ and recalling that in frequency domain $\tilde{v}(\omega) = i\omega x(\omega)$ the relation above can be rewritten as

$$x(\omega) = Y(\omega)\frac{F_{th}(\omega)}{i\omega} \tag{6.2}$$

According to the fluctuation-dissipation theorem, power spectrum of the thermal fluctuation force $S_F(\omega)$ is given by

$$S_F(\omega) = 4k_bT\,\mathrm{Re}\left[Z(\omega)\right] \tag{6.3}$$

where k_b is the Boltzmann constant and T is the temperature of the system.

This relation, together with Eq 6.2 allows us to compute the power spectral density for the mass position:

$$S_x = |Y|\frac{S_F}{\omega^2} = \frac{4k_bT}{\omega^2}\mathrm{Re}\left[Y(\omega)\right]$$

In our systems, the dissipative forces causing thermal noise are mainly due to internal damping of the material composing the mirrors and their suspensions. An effective model to describe this effect is an extension of Hooke law [9]:

$$F = k\left[1 + i\phi(\Omega)\right]x \tag{6.4}$$

where the imaginary coefficient ϕ, the *loss angle*, accounts for the dissipation of the system, introducing a delay between the force applied and the displacement. The corresponding spectral density is:

$$S_x = \frac{4k_bTk\phi}{\phi^2k^2 + \omega\left(k - M\omega^2\right)^2} \tag{6.5}$$

which, above the resonance, can be approximate as

$$S_x = \frac{4k_bT\phi\omega_0^2}{M\omega^5} \tag{6.6}$$

where ω_0 is the angular frequency at resonance.

6.1 Pendulum thermal noise

We used this model to compute the pendulum thermal noise spectrum for the suspended injection bench (SIB1) and the end mirror mode cleaner (MC). The elastic constant of the pendulum is the sum of the lossless constant provided by gravity

$$k_g = \frac{Mg}{L}$$

(where M is the mirror mass and L is the wire length) and a smaller constant which originates from the wire elasticity and is affected by losses

$$k_{el} = \frac{N_w\sqrt{T_wEI}}{2L^2}\left(1 + i\phi_w\right)$$

with N_w number of wire, E wire material Young module, L wire length, I moment of inertia of the wire cross section, T_w tension of each wire and ϕ_w is the loss angle of the wire. Since $k_g \gg k_{el}$ we have

$$k_{tot} \approx k_g\left(1 + i\frac{k_{el}}{k_g}\phi_w\right)$$

The loss angle is

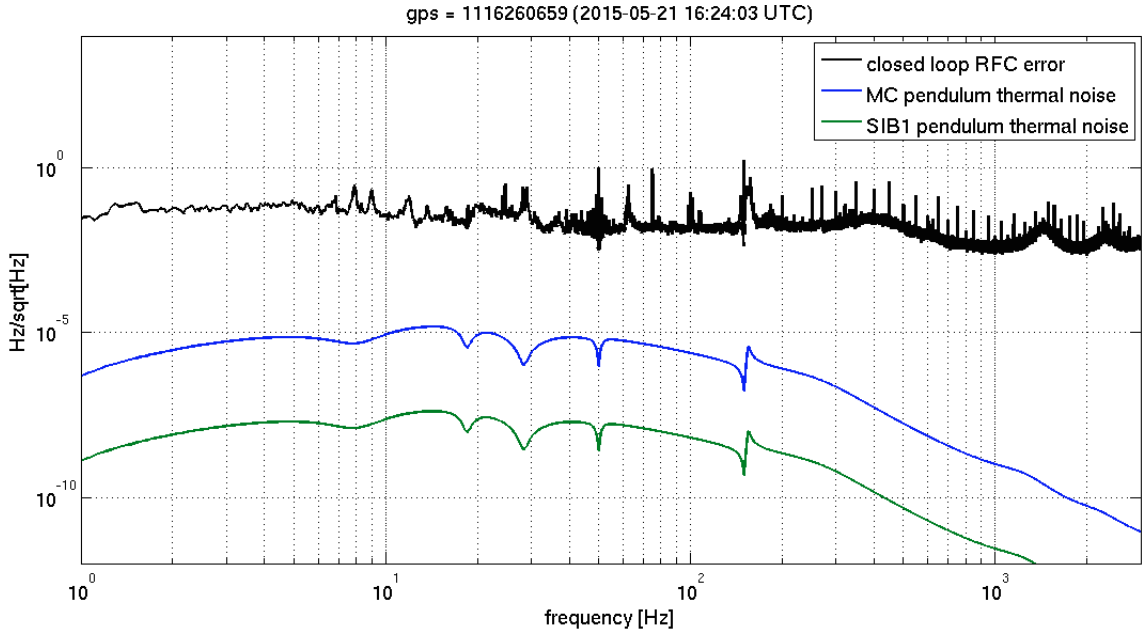

Figure 7: Pendulum thermal noise contributions of SIB1 and MC compared with the RFC error signal

$$\phi_p = \frac{k_{el}}{k_g}\phi_w = \frac{N_w\sqrt{T_w EI}}{2gLM}\phi_w$$

The ratio $\frac{k_{el}}{k_g}$ usually referred to as *dilution factor* is a measure of the loss reduction achieved using a pendulum instead of a spring made of a material with the same loss angle ϕ_w of the pendulum wire. The thermal spectrum above resonance is obtained by putting the pendulum loss angle ϕ_p in Eq. 6.6:

$$S_x = \frac{4k_b T\phi_p\omega_0^2}{M\omega^5} \tag{6.7}$$

We computed the square root of this quantity for both the mode cleaner end mirror and the injection bench to find the amplitude spectral density of the displacement. We used the following parameters:

		SIB1	MC
Weight	M	198 kg	3.4 kg
Number of wires	N_W	3	2
Wire length	L	0.7048 m	0.555 m
Wire's cross section moment of inertia	I	$5.153 \cdot 10^{-13}$ m^4;	$2.485 \cdot 10^{-17}$ m^4
Wire material		Maraging steel 250	C40 steel
Wire material modulus of elasticity	E	$2.1 \cdot 10^{11}$Pa	$2.2 \cdot 10^{11}$Pa
Wire's losses	ϕ_w	$6 \cdot 10^{-5}$	$1.9 \cdot 10^{-4}$

The dilution factor of the SIB1 and the MC are respectively $9.2 \cdot 10^{-6}$ and $7.3 \cdot 10^{-4}$. By multipling them for the respective material loss angles we find $\phi_p^{IB} = 6 \cdot 10^{-11}$ and $\phi_p^{MC} = 1.4 \cdot 10^{-7}$. The two contributions and their incoherent sum are compared with the RFC error signal in Fig.7.

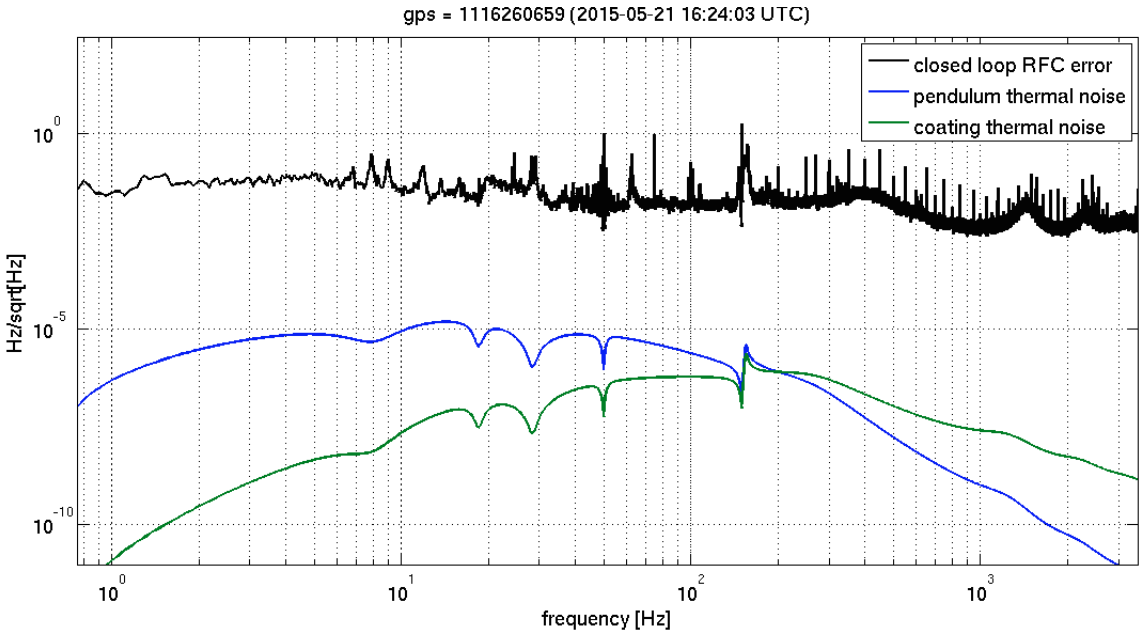

Figure 8: Pendulum and coating thermal noise spectrum compared with RFC error signal

6.2 Coating thermal noise

Starting from the fluctuation-dissipation theorem, the mirror thermal noise can be computed by means of a direct approach [10] in which the observable affected by thermal noise x(t) is defined as the displacement of the mirror surface u(r,t) as sensed by the impinging laser beam whose intensity in our case has a Gaussian profile I(r).

$$x(t) = \int I(r)u(r,t)dS \tag{6.8}$$

To compute the thermal noise spectrum we could imagine to apply on the mirror, for each frequency, a sinusoidal force $F(r,t)$ with the same intensity distribution of the laser beam. The admittance of this system Y is

$$Y(\omega) = \frac{i\omega x(\omega)}{F(\omega)} = \frac{v(\omega)}{F(\omega)}$$

its real part will account for the dissipation of the system

$$Re[Y] = Re\left[\frac{v(\omega)F^*}{F(\omega)^2}\right] = \frac{W_{diss}(\omega)}{F(\omega)^2}$$

Thanks to the fluctuation dissipation theorem, the spectrum of the mirror surface motion induced by thermal noise is found to be

$$S_x = \frac{4k_bT}{\omega^2}Re[Y] = \frac{4k_bT}{\omega^2}\frac{W_{diss}(\omega)}{F(\omega)^2} \tag{6.9}$$

where W_{diss} is dissipated energy. For a mirror with loss angle ϕ the dissipated energy is given by:

$$W_{diss} = \omega\phi U_{max} \tag{6.10}$$

where U_{max} is the maximum energy stored in the mirror during an oscillation. This corresponds to:

$$U_{max} = \frac{1-\sigma^2}{2\sqrt{\pi}E_0 w}F(\omega)^2 \tag{6.11}$$

where σ is the Poisson ratio, E_0 the mirror Young modulus and w the laser beam radius.

Finally we can find the mirror thermal noise spectrum

$$S_x = \frac{4k_bT}{\omega}\frac{(1-\sigma^2)}{2\sqrt{\pi}E_0 w}\phi \tag{6.12}$$

It has been observed that the main contribution to the mirror total thermal noise is due to the tiny reflective coating layer on the mirror surface. In fact when a gaussian force is applied on a mirror most of the stored energy is concentrated on the surface and the losses of the coating material which has to be highly reflective are quite lager than the one of the substrate. The coating thermal noise is given by the following expression [13]:

$$S_x = \frac{8k_bT}{\omega}\frac{(1+\sigma)(1-2\sigma)t}{\pi E_0 w^2}\phi_c$$

We computed the square root of this quantity for both the mode cleaner end mirror and the injection bench to find the amplitude spectral density of the displacement using : $\sigma = 0.17$, $E_0 = 7 \cdot 10^{10}$Pa, $w_{IB} = 0.005$ m, $w_{MC} = 0.01$ m, $\phi^c_{IB} = 5 \cdot 10^{-4}$, $\phi^c_{MC} = 5 \cdot 10^{-4}$, coating thickness $t_{IB} = 1.8 \cdot 10^{-}6$ m, coating thickness $t_{MC} = 6.5 \cdot 10^{-}6$ m. The total coating thermal noise is compared with the pendulum thermal noise and the RFC error signal in in Fig.8

7 RFC length noise

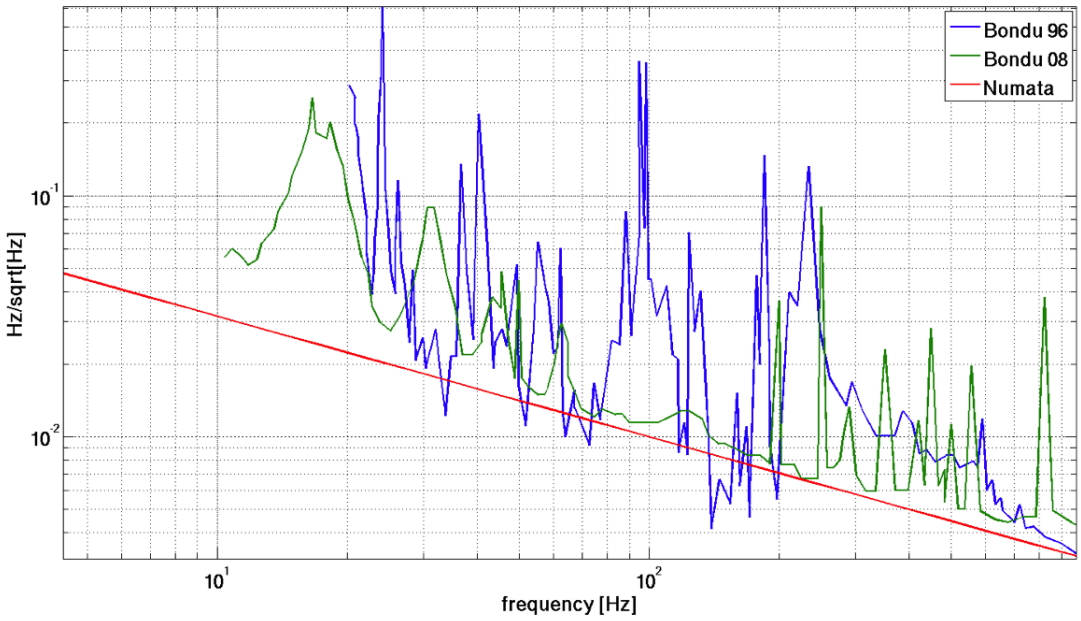

Figure 9: Theoretical estimated RFC length noise (red line) is compared with two different experimental measurements

The rigid reference cavity, used to stabilize the laser at low frequencies, is affected by a length noise which projects on the RFC error signal. An upper limit for this noise has been obtain in [12](Bondu '96). Two RFCs have been used: a laser was locked to one of them and the other was used as a reference to measure the frequency

stability. The error signal spectrum of the measurement cavity in Fig.9 (blue line) is the sum of the two RFC cavity noise. Another measurement of the RFC noise has been performed using as reference a very stable laser obtained by means of the VIRGO second stage of frequency stabilization [3](Bondu '08). The spectral density is plotted in Fig.9 (green line) and seems to be in agreement with the first measurement.
A theoretical estimation of the RFC length noise has been done in [11](Numata)assuming that the noise originates from thermal fluctuations. The contribution of the spacer and the mirrors (coating and substate) has been numerically evaluated. The thermal noise has been found to be

$$n_{RFC} = \frac{10^{-1}}{\sqrt{f}} \frac{Hz}{\sqrt{Hz}} \tag{7.1}$$

This estimation is plotted in Fig.9 (red line) together with the two measurements. The theory shows a good agreement with the floor of both experimental results. We will use the estimation given by Numata as RFC length noise in our noise budget. The projection of this noise on the RFC error signal is shown in Fig.10 and it seems to be the limiting noise in the frequency region between 50 and 120 Hz.

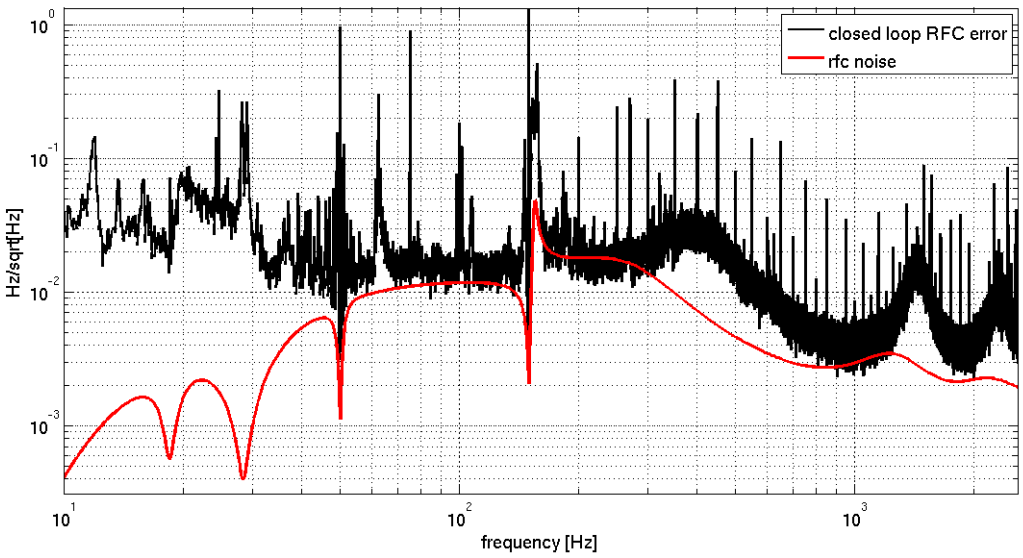

Figure 10: RFC length noise projection on the RFC error signal.

8 Angular control noise

In order to keep the IMC aligned with respect to the laser, the angular degrees of freedom of the MC end mirror and the suspended injection bench are controlled using two different techniques. The Local Control uses optical levers as position sensors referred to the ground. It provides information only on the position of one single mirror and not on the laser beam position with respect to it. Moreover, using the ground as reference, it can be affected by seismic noise. The automatic alignment, on the other hand, uses the fact that a cavity misalignment generates higher order modes. The amount of higher order modes produced is measured, using modulated light and quadrant photodiodes, and provides information on the cavity alignment. Three quadrants are used: two placed in reflection with a Gouy phase shift of 90 deg, modulated at 22 MHz and a DC quadrant placed in transmission of the MC end mirror. The sensitive degrees of freedom to be controlled are θ_x, θ_y, θ_z for the SIB1 and θ_x, θ_y for the MC. The relation between their values and the quadrant signal is expressed by the optical matrix. This is measured by means of sinusoidal noise injections at 2 Hz on the actuators which allows

to measure the transfer function between each degree of freedom of the mirror position and the quadrant signal. The correction matrix is found inverting the measured optical matrix. Then it is filtered and the corrections are sent to the actuator.
Local controls are used to stabilize the mirrors during the lock acquisition and to reduce their angular displacement below some tenths of microradians in order to reach the linear regime of the Automatic Alignment error signals. Two different control schemes are possible: a *fast control* which uses only global signal with a bandwidth of tens of Hz and a *drift control* where the global control are used with a control bandwidth of few mHz while at higher frequency local control are used. In order to measure the noise contribution of the angular control noise to RFC error, we measure the transfer function between the correction applied to the marionetta and the RFC error signal. This has been done by means of a noise injection on the marionetta. The transfer functions for the three injection bench degrees of freedom θ_x, θ_y, θ_z are shown in Fig.11

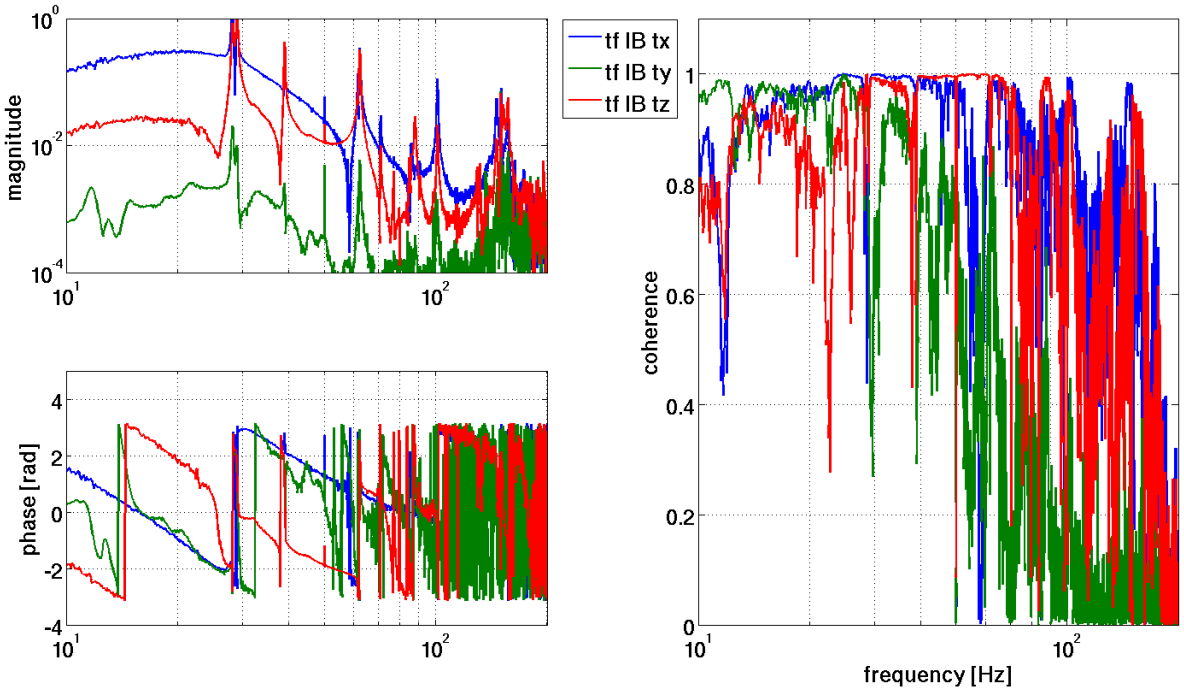

Figure 11: Transfer functions between the correction applied to the marionetta and the RFC error signal for the 3 degree of freedom of the injection bench

The contribution of the angular control noise of the injection bench to RFC error signal is found by multiplying the spectrum of the correction signal in normal condition with the absolute value of the measured transfer function.

$$N_{\text{proj}}(f) = |TF(f)|_{\text{with noise}} \cdot |ASD(f)|_{\text{no noise}} \tag{8.1}$$

As it can be seen in Fig.12 the IB angular control noise represents the limiting noise in the RFC error signal up to 40 Hz.

9 Jitter noise

The beam pointing noise, usually referred to as jitter noise, consists in a shift or a tilt of the input beam axis with respect to the IMC cavity axis. A jitter of the beam which enters the interferometer couples with a possibile

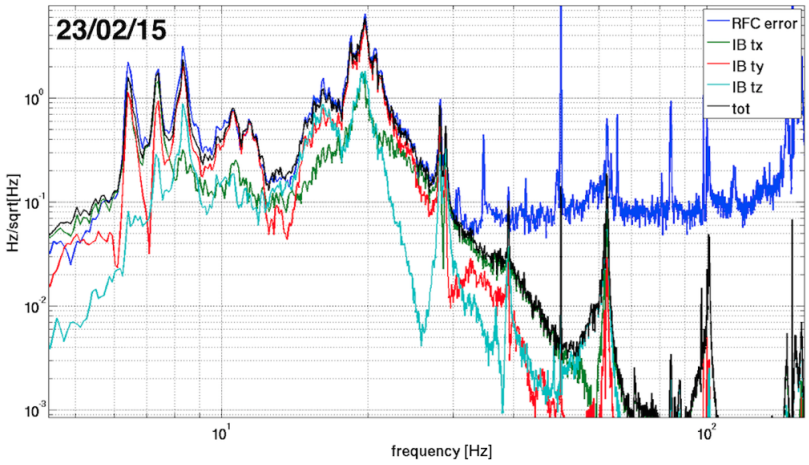

Figure 12: Injection Bench angular control noise projection

asymmetry between its arms causing a phase noise. For that reason the injection system has to deliver a beam with specific requirements in terms of jitter. A sensing system composed by two quadrant photodiode is used to monitor the shift and the tilt of the beam at the IMC input [14]. A beam pick-off is taken before the IMC and it is sent to two quadrants which are placed at a distance producing a Gouy phase shift of 90 deg. In this way each quadrant is sensitive only to one degree of freedom: the pure shift for the so-called Near Field quadrant and the tilt for the Far Field one. These signals are used as error signals in a feedback loop, the Beam pointing control (BPC), active in the frequency range up to 10 Hz. The correction obtained filtering the error signal, is sent to the actuators: two tip/tilt piezo mirrors placed as in Fig.13.

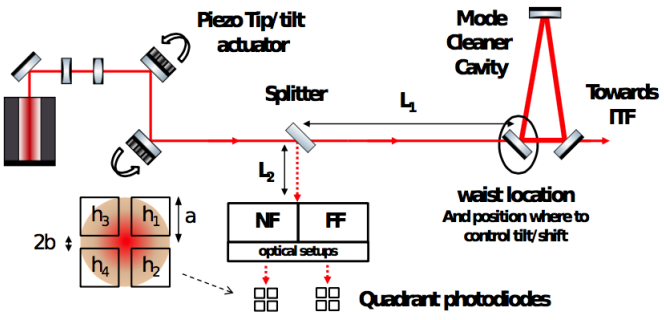

Figure 13: Beam pointing control scheme from [14]

Above the bandwidth of the Automatic Alignment loop (~ 1 Hz) the IMC acts as a filter for the beam jitter. The jitter, seen as a misalignment by the cavity, produces higher order modes which cannot resonate in it and are weakly transmitted. On the other hand in the region where the Automatic Alignment is active the cavity is kept aligned following the beam position fluctuation which are transmitted almost unchanged.
The projection on the RFC error signal has been found, as usual, injecting noise on the BPC actuators and measuring the transfer function between the jitter and the RFC error signal for all the degree of freedom: shift in x and y and tilt in θ_x and θ_y. The transfer functions have been than multiplied for the jitter signals in normal condition to find the noise projections that are shown in Fig.14.

The mechanism through which the jitter noise affects the RFC error signal is not straightforward. For example,

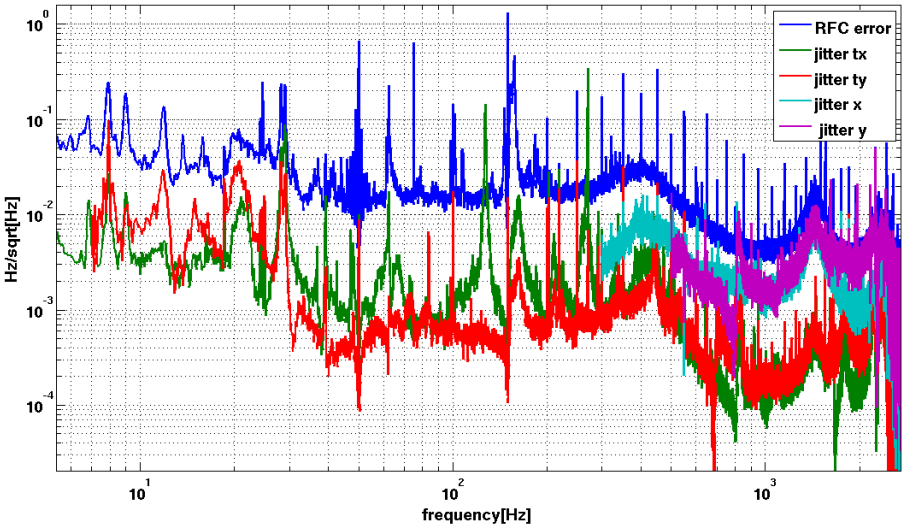

Figure 14: Jitter noise projection on the RFC error signal

in the RFC error curve there are peaks around 10 Hz explained by the noise projection of the angular control of the input bench and also seen by the BPC sensors. We found them to have a high coherence with the seismometers of the external injection bench (EIB). Since the AA quadrants on the EIB are supposed to be insensitive to seismic noise at the first order, we suppose that motion of the EIB causes a real jitter of the beam which is seen as a misalignment from the AA quadrant and then re-injected as angular control noise by their control loop. However this coupling mechanism through the AA control loop is unlikely to acts at high frequency (for example at 100 Hz where the jitter seems to be a limiting noise) because the AA loop is not active at these frequencies.
From the argument above it is evident that at low frequency, angular control noise and jitter noise can not be considered independent. For that reason they can not be summed in quadrature to obtain the total noise. A solution to avoid an overestimation of the total noise is to take into account in the sum the jitter noise projection obtained from a transfer function measured under local control.

10 Automation and total noise budget

In order to quickly compute up-to-date noise budget a MATLAB script[4] to automate the procedures described above has been implemented . It takes as input the GPS at which we want to calculate the noise budget, collects data, and produces a complete noise budget for the RFC error signal as the one shown in Fig.15.
The plot of the total noise budget gives an overview on the contribution to total frequency noise of the different noises taken into account in this analysis. Some of them are so small that it is not worth considering them for commissioning purposes. In Fig.16 and Fig.17 the frequency noise budget is shown for the low and high frequency region, respectively and only the relevant noises have been plotted.
In this note we just plotted a particular frequency noise curve. It is interesting to notice how frequency noise has been decreased in the past months thanks to the commissioning activity until it reached the requirement of 1 Hz RMS. The improvement of the noise in the past months is shown in Fig.18
Noise transfer function, needed to project angular and jitter control noise are likely to change during commissioning and should be often re-measured. The noise injection process to compute such transfer functions has been also automated. A dedicated Photodiode Readout (PR) process [15], CaNoise, is used to generate

[4]The MATLAB script can be found in /olusers/virgorun/RFC_NoiseBudget/RFC_NoiseBudget.m

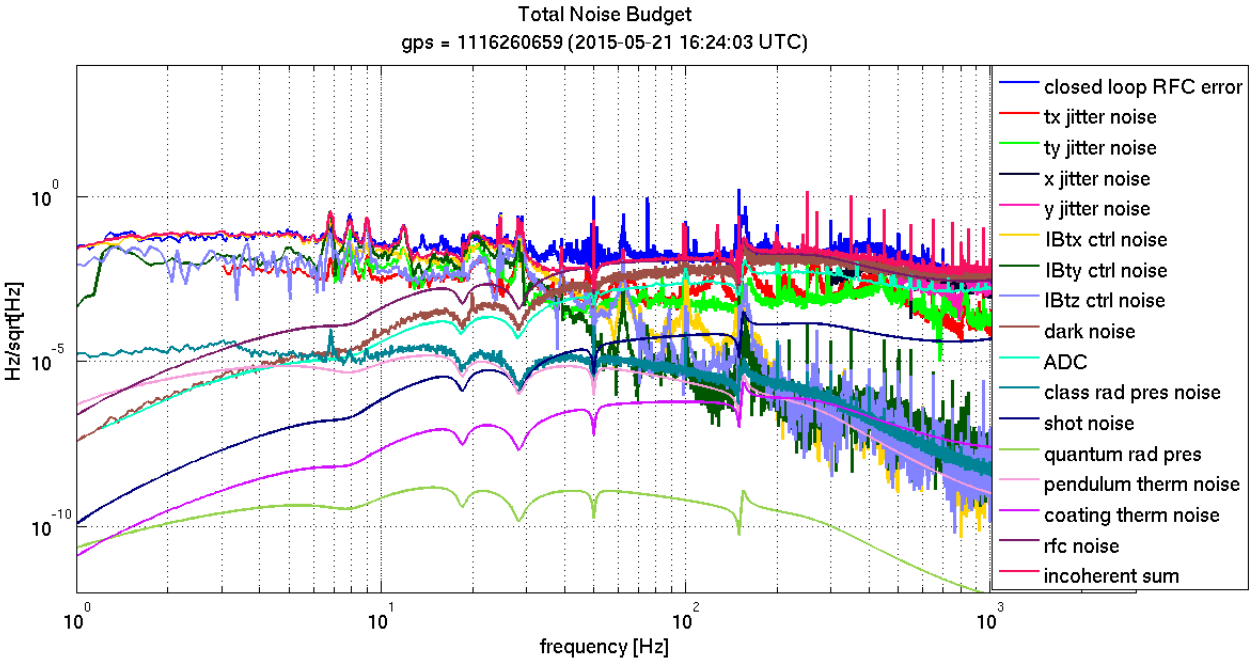

Figure 15: Example of a noise budget produced using the MATLAB script

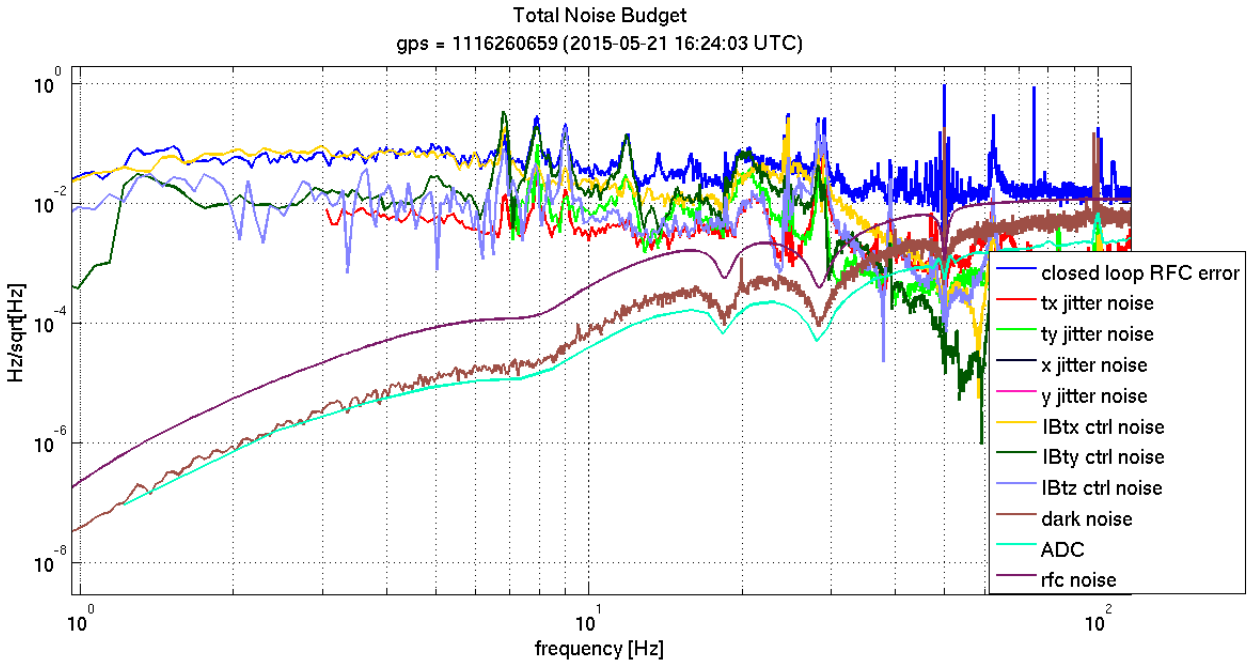

Figure 16: Noise budget of the RFC error signal at low frequency where only the most relevant noise are plotted

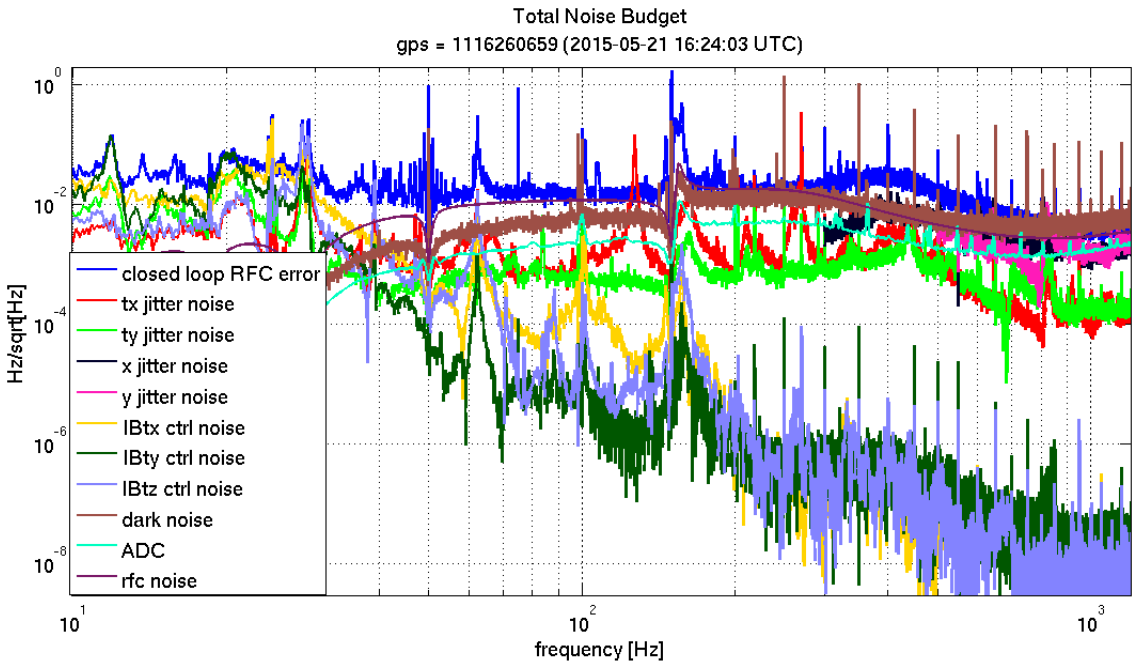

Figure 17: Noise budget of the RFC error signal at high frequency where only the most relevant noise are plotted

and shape the noise which is then sent to the various DSPs by cm commands. A Python script[5] handles this procedures and records the GPS of the injections in a logfile. Such gps are then inserted in another MATLAB script to work out up-to-date transfer functions.

[5]The Python script can be found in /virgoData/NoiseInjections/INJ/inject.py

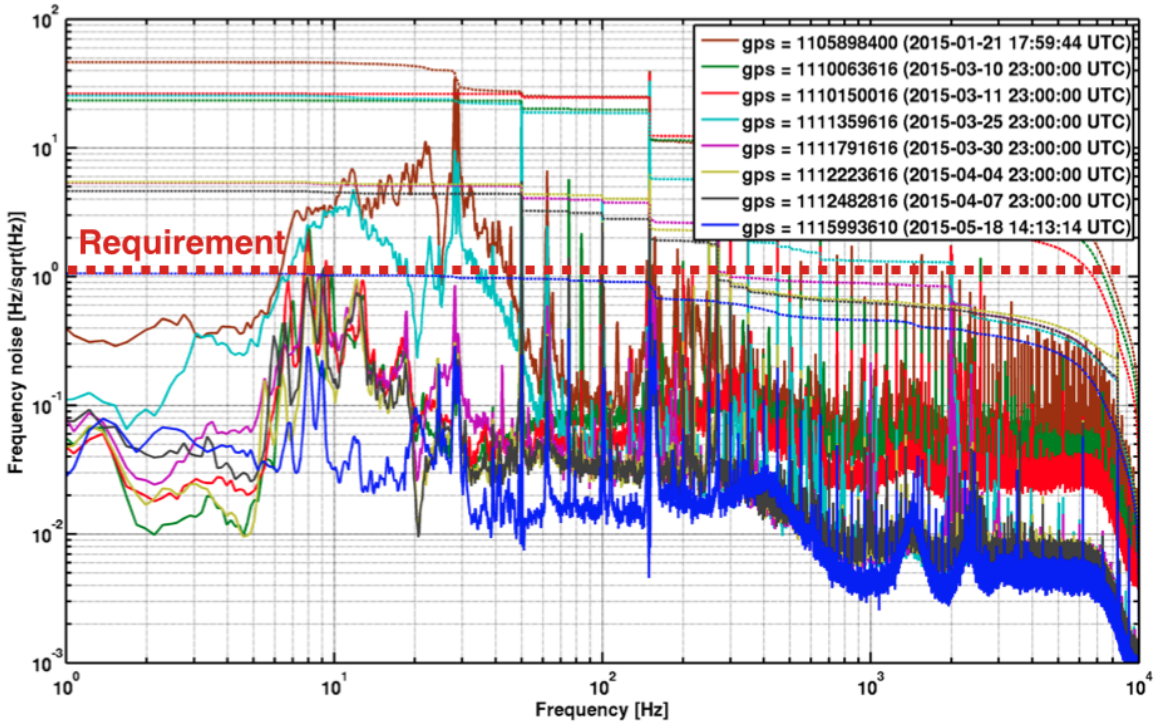

Figure 18: Improvement of the RFC error signal up to the requirement of 1 HZ RMS

References

[1] The Virgo Collaboration "Advanced Virgo Technical Design Report ", VIR-0128A-12. Pag. 93 2

[2] E. Calloni, G.Vajente "Conceptual design of the second stage of frequency stabilization for Advanced Virgo ", VIR-0013C-12 2

[3] F. Bondu, L' interferometre Virgo: proprietes optiques, stabilisation en frequence du laser, Memoire d' habilitation a diriger des recherches, Observatoire de la Cote d' Azur (2008) 2, 14

[4] E. Genin on behalf of the INJ team, "INJ status @ July 2015 coll. meeting", VIR-0311A-15 8

[5] B. Canuel, E. Genin, J. Marque, P. Benoit, "Reference Cavity characterization", VIR-0231A-13 4

[6] B. Swinkels, "Requirements on sensing noise for the Pound-Drever-Hall technique for the lock of the arm-cavities", VIR-0467A-12 7

[7] E. Genin on behalf of the INJ team, "INJ status @ July 2015 coll. meeting", VIR-0311A-15 8

[8] H.B.Callen and R.F.Green, Phys. Rev. 86, 702 (1952) 9

[9] P. R. Saulson, Phys. Rev. D 42 (1990) 10

[10] Yu. Levin, Phys. Rev. D 57, 659 (1998). 12

[11] K. Numata, A. Kemery, and J. Camp, Physical Review Letters 93 (2004) 14

[12] F. Bondu et al., Opt. Lett. 21, 582 (1996) 13

[13] Chalermsongsak et al. "Broadband Measurement of Coating Thermal Noise in Rigid Fabry-Perot Cavities", *Metrologia* 52 17 (2015) 13

[14] B.Canuel et al. "A sub nrad beam pointing monitoring and stabilization system for controlling input beam jitter in GW interferometers" Appl.Opt. 53 (2014) 2906 16

[15] M.Evans et al., The Pr server Documentation, (https://vpm.virgo.infn.it:40000/doc/CaNoise/PrDoc_Lx.pdf) 17